Revised manuscript (clean version) Click here to view linked References

New insights into the concentration-dependent regulation of membrane biofouling formation via continuous nanoplastics stimulation

Xinhui Liu[a], Yu Yang[a, *], Satoshi Takizawa[b], Nigel J.D. Graham[c], Chao Chen[a], Jian Pu[d, e], How Yong Ng[f,g]

[a] School of Environment, Beijing Normal University, Beijing, 100875, China

[b]Department of Urban Engineering, Graduate School of Engineering, The University of Tokyo, 7-3-1 Hongo, Bunkyo-ku, Tokyo 113-8656, Japan

[c]Department of Civil and Environmental Engineering, Imperial College London, South Kensington Campus, London SW7 2AZ, UK

[d]Institute for the Advanced Study of Sustainability, United Nations University, Jingumae 5-53-70, Shibuya-ku, Tokyo 150-8925, Japan

[e]Institute for Future Initiatives, The University of Tokyo, Tokyo 113-0033, Japan

[f]Center for Water Research, Advanced Institute of Natural Sciences, Beijing Normal University, Zhuhai, 519087, China

[g]National University of Singapore Environmental Research Institute, 5A Engineering Drive 1, 117411, Singapore

[*] **CORRESPONDING AUTHOR**

Yu Yang E-mail address: yangyu@bnu.edu.cn

Abstract

The release of nanoplastics (NPs) into the environment is growing due to the extensive use of plastic products. Numerous studies have confirmed the negative effects of NPs on microorganisms, which poses uncertainties concerning their impact on nanofiltration (NF) membrane biofouling. This study investigated the initial cell adhesion process, NF membrane biofouling kinetic processes and bacterial responses of *Pseudomonas aeruginosa* (*P. aeruginosa*) exposed to varied NPs concentrations (0–50 $mg \cdot L^{-1}$). Transcriptome analysis demonstrated that low concentration of NPs (0.1 $mg \cdot L^{-1}$) promoted bacterial quorum sensing, energy metabolism, exopolysaccharide biosynthesis and bacterial secretion systems. Correspondingly, the polysaccharide content increased remarkably to 2.77 times the unexposed control, which served as a protective barrier for bacteria to avoid the impact of NPs-induced stress. Suppressed homologous recombination, microbial metabolic potentials and flagellar assembly were detected in bacteria exposed to a high concentration (50 $mg \cdot L^{-1}$) of NPs, mainly due to the triggered reactive oxygen species (ROS) generation, genomic DNA damage, and decreased energy production. Overall, enhanced formation of the extracellular polymeric substances (EPS) and aggravated membrane flux decline were observed when NPs interacted with the membrane surface by cell secretions (low NPs levels) or cell lysis (high NPs levels). These findings shed light on understanding the microbial metabolism mechanism and membrane biofouling propensity with NPs stress at both the molecular and gene levels.

Keywords: Nanoplastics (NPs), Nanofiltration (NF), Wastewater treatment, Initial attachment, Membrane biofouling, Transcriptome analysis

1. Introduction

In recent years, the widespread manufacturing and uncontrolled disposal of plastic products has resulted in the release of a substantial amount of plastic fragments into the aquatic environment (Horton et al., 2017). These quantities of plastic debris, particularly nanoplastics (NPs), can pass through the blood-brain barrier easily and can cause a variety of adverse impacts to human health (e.g., mortality, developmental toxicity, endocrine toxicity, immunotoxicity and genotoxicity) and the ecological environment because of their ultrafine particle size and high surface-to-volume ratio (Teng et al., 2022; Wen et al., 2022). However, the increasing concentrations of NPs in wastewater are considered inevitable due to widespread anthropogenic activities and urban development. In recent research (Zhou et al., 2021), 2.82 $\mu g \cdot L^{-1}$ of polystyrene NPs were detected in the influent of wastewater treatment plants (WWTPs) using pyrolysis-gas chromatography/mass spectrometry (Py-GC/MS). However, the environmental presence of small plastic fragments may be substantially underestimated due to secondary contamination in the treatment processes, especially NPs with particle sizes in the range of a few hundred nm (Sorasan et al., 2022; Yang et al., 2023). Therefore, NP-specific treatment solutions are urgently needed to lessen their environmental risk, environmental implications and potential ecotoxicity.

Membrane filtration has been identified as an effective method for NPs removal. The pore size of NF membrane is similar to that of NPs particles, which provides good interception performance for NPs removal (Malankowska et al., 2021; Sutrisna et al., 2023). A major limitation of membrane filtration technology is the development of biofouling, which can increase the energy requirements and operational complexity of NF membranes (Cui et al., 2015). The strong adsorption ability of extracellular

polymeric substances (EPS) can facilitate the transfer of NPs from raw waters/wastewaters into the membrane biofilm, which provides an opportunity for NPs to interact with microorganisms and ultimately affects the performance of the NF process. In general, insufficient research has been undertaken to-date relating to the biofouling behavior and the factors controlling the removal of NPs by NF. Thus, more research is required to understand the impacts of NPs on the performance of the NF process, and especially concerning the related biofouling kinetic formation process.

There is currently no consensus regarding the effect of NPs on bacteria. A recent study revealed that NPs with mean diameters of approximately 75 nm might induce the production of free radicals in *E. coli* and damage the integrity of cell membranes (Wang et al., 2022). The authors also confirmed that NPs promoted the uptake of exogenous DNA by bacteria by inducing excessive formation of reactive oxygen species (ROS), activating the DNA damage-induced response (SOS response), and increasing cell membrane permeability. Exposuring to 20 and 50 $mg \cdot L^{-1}$ of polystyrene NPs significantly increased the expression of genes encoding for flagellar biosynthesis and biofilm formation in response to stress (Hu et al., 2022). An interesting discovery demonstrated that plastic leachates significantly increased the acquisition of bacterial biomass by providing more assimilable organic carbon (Sheridan et al., 2022). As an important tool for providing information on the toxicity mechanisms of contaminants to microorganisms, transcriptome analysis indicated that the polystyrene NPs upregulated glutathione metabolism and unsaturated fatty acid related genes, while downregulated genes encoding methyltransferases in *R. jostii* (Xu et al., 2022). In light of the intricate interactions between NPs and bacteria, we believe that NPs will also have a significant impact on the dynamic formation of NF membrane biofouling, thereby affecting membrane performance. To the best of our knowledge, none of the

previous research studies have explored the influence of NPs on the NF biofouling kinetic formation process.

This study aims to reveal the mechanisms of NF membrane biofouling induced by different levels of exposure to NPs. A series of filtration tests were conducted to determine the dynamic changes in the biofouling composition at different time periods. In addition, the responses of physiological features (e.g. secretion characteristics and energy metabolism features) with variations in genome were investigated using transcriptome analysis. The specific objectives of the study are to: (1) evaluate the impact and mechanism of increasing NPs concentrations (0–50 $mg \cdot L^{-1}$) on the initial attachment process and the kinetics of biofilm formation in the NF process; and (2) investigate the changes of microbial activity, energy production, and metabolic gene expressions exposed to increasing NPs concentrations. The findings of this study provide valuable insight into the biofouling behavior, metabolism and proliferation of microorganisms induced by different concentrations of NPs in the NF based process, which can be used to enhance the sustainability of the membrane filtration process.

2. Materials and methods

2.1 Materials and preparation of synthetic wastewater

The development of the NF membrane in a cross-flow filtering system was conducted using synthetic wastewater effluent based on the quality of a WWTP secondary effluent (Table S1), which has been applied in a previous study (Cui et al., 2015). As carbon, nitrogen and phosphorus sources, $Na_3C_6H_5O_7$, NH_4Cl and KH_2PO_4 were used, respectively. Before filtration, the synthetic wastewater was sterilized for 30 min at 121°C. All chemicals were acquired from Sinopharm Chemical Reagent Co., Ltd., China, unless otherwise noted.

As the most widely used plastic polymers and the main components of plastic

120 debris detected in aquatic ecosystems, polystyrene latex beads without functional
121 groups and chemical reactivity (Tianjin BasLine, China) were selected as the
122 representative NPs (~ 80 nm, Fig. S1). All experiments were performed with an NPs
123 stock solution (25 $g \cdot L^{-1}$ with no fluorescence labeling and 10 $g \cdot L^{-1}$ with blue
124 fluorescence labeling) and distilled water. The synthetic wastewater with a final
125 concentration of 0–50 $mg \cdot L^{-1}$ polystyrene NPs was prepared after diluting the NPs
126 stock solution. The concentration range refers to published NPs toxicology tests, which
127 aimed to unravel the response of *Pseudomonas aeruginosa* (*P. aeruginosa*) to
128 increasing concentrations of NPs (Enfrin et al., 2021; Song et al., 2022; Yang et al.,
129 2022). Prior to usage, the feed and stock solutions were sonicated for 30 min to promote
130 the uniform distribution of NPs particles.

131 *P. aeruginosa* (PAO1) is a gram-negative, rod-shaped *Proteobacteria*-class
132 bacterium widely found in membrane biofilms (Luo et al., 2022). *P. aeruginosa* was
133 cultivated overnight at 37°C and 180 rpm in LB (Luria-Bertani) broth (Table S2) to a
134 concentration of ~ 2×10^9 CFU (colony forming unit)$\cdot mL^{-1}$ and an optical density
135 ($OD_{600\ nm}$) of 1.0. After 2 min of centrifugation at 12,000 rpm, *P. aeruginosa* was
136 re-suspended in the prepared synthetic wastewater and used as inoculum in the
137 cross-flow NF system.

138 **2.2 EPS composition analysis, cellular motility and adhesion experiment**

139 *P. aeruginosa* were grown at 37°C in Erlenmeyer flasks containing 50 mL of LB
140 broth amended with NPs at final concentrations of 0, 0.1, 1, 10 or 50 $mg \cdot L^{-1}$ (referred to
141 as, R0, R0.1, R1, R10 and R50). Loosely bound EPS (LB-EPS) and tightly bound EPS
142 (TB-EPS), which play different roles in microbial aggregates, were analyzed using a
143 heating method after 12 h incubation (Wu et al., 2023). Swarming distance and colony
144 area were recorded to explore the effect of NPs exposure on cellular motility, and

detailed information can be found in a previous study (Wang et al., 2023). Transmission electron microscopy (TEM, Hitachi-HT7700, Japan) was used to observe the bacterial morphology and to clarify the NPs-cell interaction sites.

The static adhesion experiment was carried out according to previous research studies with little modification (Nikkola et al., 2013; Yu et al., 2012). Firstly, the commercial NF270 membrane (FilmTec, America) was cut into areas of 1×1 cm^2 and immersed in a 40% ethanol solution for 12 h to remove organic impurities (Heffernan et al., 2013). After 12 h of soaking in Milli-Q ultrapure water, NF270 membranes were sterilized for 30 min with ultraviolet lamp irradiation. The membrane was then placed on the bottom of a 6-well tissue culture plate, to which was added 5 mL of fresh LB broth (containing 5×10^7 *P. aeruginosa* cells and 0–50 $mg\cdot L^{-1}$ NPs per well). The entire experimental procedure was carried out on a clean bench, and all static bacterial adhesion experiments were conducted in triplicate. After 1, 2, 3 and 4 h (i.e., short term) and 12, 24 and 36 h (i.e., long term) of static culture at 37°C, membranes were rinsed gently with PBS buffer to remove loosely attached bacteria. The bacteria adhering to the membrane surface were fully dispersed and suspended in PBS buffer by ultrasound water bath extraction methods. Serial dilutions were made in sterile water, and 100 μL of each dilution was plated onto LB agar plates. The number of colony forming units was estimated by multiplying the number of colonies by the corresponding dilution factor after 12 h of static culture at 37°C. The tapping mode of atomic force microscopy (AFM, Dimension Icon, America) and contact angle measurement device (Dataphysics, OCA25, Germany) were utilized for membrane roughness and contact angle (representing the surface hydrophilicity) determinations after static adhesion experiments.

2.3 Set-up and operation of NF systems

Prior to filtration, the commercial NF270 membrane (FilmTec™, China) was stored in a 1.5% $NaHSO_3$ solution to moisten the membrane, recover flux and inhibit bacterial growth. The basic membrane properties were shown in Table S3. The membrane filtration system was comprised of four parallel cross-flow cells positioned in a cascade configuration (Fig. S2). To obtain stable water flux prior to biofouling experiments, membranes were compacted overnight with distilled water at a constant pressure of 0.8 MPa. The operating pressure was 0.6 MPa, and the feed water flow rate was 45 liters per hour (LPH). The permeate flow was determined by recording the weight of permeate collected every 30 min using a computer connected electronic scale. Both the permeate and the concentrate were returned to the feed tank to maintain a constant feed water quality.

2.4 Biofouling experiments under NPs stress

Prior to the insertion of the NF membrane and biofouling, the entire system was disinfected with anhydrous ethanol and cleaned with sterile deionized water, respectively. After achieving a stable flow, 5.0 L of synthetic wastewater was used to replace the deionized water with the addition of NPs and supplemented with *P. aeruginosa* strains to obtain a final bacterial concentration of 10^7 CFU·mL^{-1}. After biofouling formation, the NF membrane was removed, rinsed with sterile deionized water to eliminate suspended bacteria, and then stored at -20°C prior to analysis.

2.5 Biofouling component analysis

At the end of each filtration test, the membrane surface properties of biofouled membranes were determined. Extracellular polymeric substances (EPS) of the biofilm were isolated by the ultrasonication-centrifugation method (Min et al., 2022). The phenol-sulfuric acid method and Bradford protein assay kit (Beyotime, China) were used to determine the polysaccharide and protein contents, using glucose and bovine

serum antigen (BSA) as a standard, respectively. The bacterial activity in the fouling layer was assessed using the BacTiter-Glo^{TM} microbial cell viability assay in accordance with the manufacturer's protocol (Promega, America). All experiments were conducted in triplicate.

The deposited foulants on the membrane surface were analyzed by the Fourier transform infrared spectroscopy (FTIR, Thermo Scientific Nicolet iS20, America) with an attenuated total reflection (ATR) accessory. Changes in the chemical composition of the biofouled layers were studied using the X-ray photoelectron spectroscopy (XPS, Thermo Scientific K-Alpha, America). The live/dead cell viability was evaluated using a Leica fluorescence microscope (Leica TCS SP8, Germany). Surface and cross-section morphologies of biofilms were recorded using a field emission scanning electron microscope (FESEM, Hitachi, Japan).

2.6 Enzyme activity assays and transcriptome analysis

Intracellular ROS of *P. aeruginosa* was measured by a Reactive Oxygen Species Assay Kit (DCFH-DA, Solarbio, China). Bacterial enzyme activity assays of catalase (CAT) and superoxide dismutase (SOD) were measured using the Catalase Activity Assay Kit (Solarbio, China) and Superoxide Dismutase Activity Assay Kit (Solarbio, China), respectively. The release of lactate dehydrogenase (LDH) was measured using an LDH Assay Kit (Solarbio, China) according to the manufacturer's protocol. Biofilm exposure to 0, 0.1 and 50 mg·L^{-1} NPs (i.e., R0, R0.1 and R50) were sampled at the biofilm growing stage (12 h), which was preserved at -80°C and delivered to Sangon Biotech (Shanghai, China) for RNA extraction and sequencing, to explore the transcriptional changes of *P. aeruginosa* in response to low and high NPs concentrations. The quantity and quality of RNA were confirmed by NanoDrop2000 and Agilent2100, respectively. Details of the RNA sequencing and bioinformatics

analytical method have been explained in a previous study (Liu et al., 2023). The transcripts were annotated with the Kyoto Encyclopedia of Genes and Genome (KEGG) genes and associated pathways (https://www.genome.jp/kegg/) (Xu et al., 2021). Differentially expressed genes (DEGs) between control and NPs-treated groups were chosen as $|\log_2 FC|$ of the Fragments Per Kilobase Million (FPKM) value > 1.0, *p*-adjust < 0.05 (Ban et al., 2023). For validation of the transcriptome data, three functional genes encoding extracellular polysaccharide biosynthesis (*pslA*, *pelA* and *algD*) were selected for real-time quantitative PCR (RT-qPCR). The total RNA of *P. aeruginosa* was extracted using the RNAprep Pure Cell/Bacteria Kit (TIANGEN, China) and reversed transcribed using the FastKing RT Kit (With gDNase) (TIANGEN, China). After that, RT-qPCR analysis was performed using SuperReal PreMix Plus (SYBR Green) (TIANGEN, China) with a three-step procedure: 15 min of initial denaturation at 95°C, followed with 10 s denaturation at 95°C, 20 s annealing at 60°C, and 30 s extension at 72°C for 40 cycles. The primers were designed by Sangon Biotech (Shanghai, China), and additional information is shown in the SI (Table S4). All samples were normalized to the expression of the housekeeping gene *rpoC* via the $2^{-\Delta\Delta C_T}$ method (Zhang et al., 2020a).

2.7 Statistical analysis

Redundancy analysis (RDA) and principal component analysis (PCA) were performed to delineate the comprehensive relationships between the biological factors of fouling and the performance indicators of the fouled membranes. In this study, a *p*-value < 0.05 is regarded as statistically significant. One-way analysis of variance (ANOVA) and Tukey's *post hoc* test were used to determine the significance and were indicated by letters.

3. Results and discussion

3.1 Increased EPS secretion, cellular motility and membrane roughness facilitated initial attachment

Extracellular polymeric substances (EPS) possess not only an important role in the initial adhesion of cells to the membrane surface, but also are highly engaged in biofilm formation and stability (Bereschenko et al., 2010; Jafari et al., 2020; Luo et al., 2022). Two main EPS components (i.e., polysaccharide and protein) of the bacteria, which were exposed to increasing NPs concentrations, were determined (Fig. 1a-b). The NPs treatment significantly increased the contents of polysaccharide and protein in the total EPS by 30.8%–61.8% and 10.4%–15.1%, respectively ($p < 0.05$). Interestingly, the content of polysaccharide in LB-EPS and protein in TB-EPS increased with higher NPs exposure. In comparison, the content of polysaccharide in TB-EPS and protein in LB-EPS increased more significantly under lower NPs exposure. A swarming ability test was conducted to explore the effect of NPs on cellular motility (Fig. 1c). The swarming distance peaked after 12 h of incubation, when the colony diameter and area were significantly extended by 14.3%–47.8% and 33.7%–100.8%, respectively, after NPs exposure. Consistently, a recent study also indicated that bacteria with flagella (especially sticky flagella) impacted the initial attachment on plastics, and exhibited a more rigid attachment layer (Zhang et al., 2023). Pure bacteria were used for TEM observations to further explore whether NPs damaged the cell membrane or entered the cell (Fig. 1d). The TEM images showed that the untreated *P. aeruginosa* had a smooth surface, with a tightly bounded cell membrane and cell wall. Since the size of NPs (~ 80 nm) was much smaller than that of an individual microorganism, NPs particles were shown to pass easily through biological barriers and entered the intracellular region. Surface-attached and internalized plastic particles will eventually cause various cytotoxic effects on *P.*

aeruginosa, affecting their growth and viability. The cell wall was separated from the cytoplasmic membrane, but intact in R10. With higher NPs exposure in R50, the damage of cell wall and membrane with release of cytoplasmic material (i.e., plasmolysis effect) was also observed. Therefore, the penetration of NPs in *P. aeruginosa* accelerated the destabilization of the cell wall and membrane, possibly through inducing the overproduction of ROS in its interior (Tamayo et al., 2014). In a previous study, however, it was reported that NPs particles were firmly attached to the microbe surface in a sequencing batch reactor (SBR), with no NPs (100 nm) entering into or damaging the cell membrane from confocal laser scanning microscopy (CLSM) images (Song et al., 2022). The different conclusions are reasonable, as the toxicity of NPs on bacteria is variable due to species differences.

Membrane biofouling at the early stage is substantially governed by bacterial attachment (Jiang et al., 2022). According to the static adhesion experiments, the number of bacteria adhering to the membrane surface was significantly increased under NPs exposure, mainly due to increased EPS secretion and cell motility, as previous discussed (Fig. S3). Notably, more adherent cells were detected with higher NPs exposure at the initial time of 1 h (from 1.15-fold at 0.1 $mg \cdot L^{-1}$ to 3.48-fold at 50 $mg \cdot L^{-1}$), compared to the control. The AFM tapping mode 2D and 3D images (Fig. 1e-g) and contact angle (Fig. 1j) of the membrane surface after the short-time (1 h) adhesion experiment showed that the hydrophobic NPs particles tended to strongly adhered to the polymeric membrane surface, which contributed to bacterial adhesion by increasing the membrane roughness and hydrophobicity. EPS quantification of long-term (12–36 h) adhesion experiments showed that polysaccharide was more

293 significantly affected by NPs, although in total mass terms a higher protein content was
294 determined (Fig. 1h-i). Generally, polysaccharide plays an important role in bacterial
295 adhesion and nutrients retention, whereas protein provides carbon sources for the
296 development of biofilm and maintains the stability of biofilm structure (Shi et al., 2017).
297 Overall, these results implies that NPs promoted the initial attachment process by
298 increasing membrane roughness, activating cellular motility, and promoting EPS
299 secretion (Fig. 1k). It is worth noting that the enhanced direct attachment of bacteria on
300 the membrane surface subsequently results in a significant permeate flux decline in the
301 NF systems, which is discussed in the following sections.

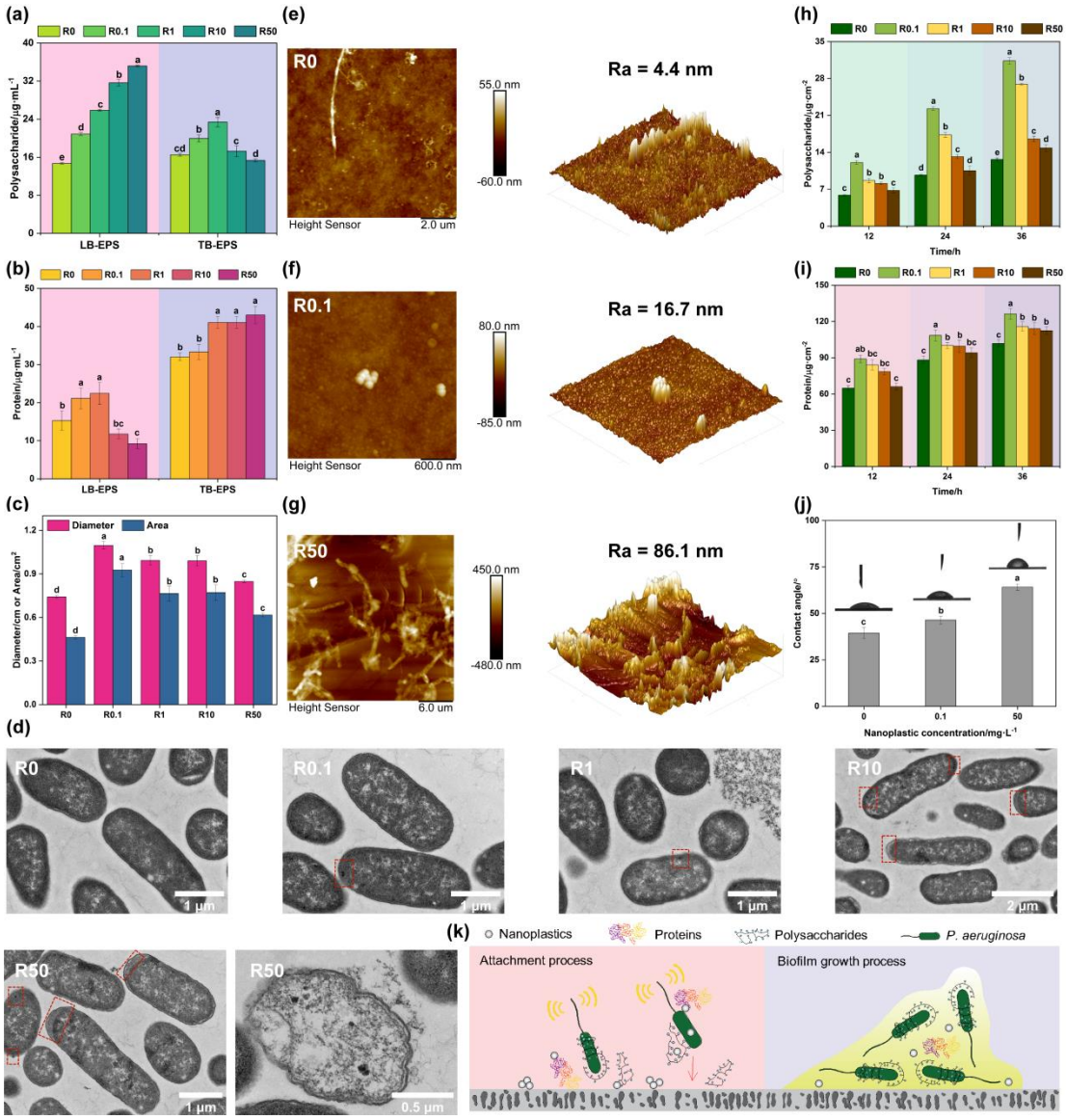


Fig. 1. The concentrations of polysaccharide (a) and protein (b) in LB-EPS and TB-EPS after 12 h incubation; ANOVA analysis and Tukey's *post hoc* test were performed, lowercases indicate significant differences among treatments ($p < 0.05$); the cellular motility variation under the exposure of increasing NPs concentrations (c); TEM images of *P. aeruginosa* untreated or treated with NPs after 12 h incubation (d); AFM images (e-g) and contact angles (j) of the membrane surface after short-term (1 h) adhesion experiments; polysaccharide (h) and protein (i) contents of membrane biofouling layers after long-term (12–36 h) adhesion experiments; schematic representation of the initial attachment process of *P. aeruginosa* exposed to NPs, the increased cellular motility, membrane roughness, and the protein and polysaccharide secretion accelerated bacterial adhesion (k).

3.2 The trapped NPs particles aggravated membrane biofouling with suppressed cell viability

Synthetic wastewater inoculated with *P. aeruginosa* was used to induce biofouling on the NF membrane. As shown in Fig. 2a, the experiments with the addition of different NPs concentrations showed similar flux declines (76.2%–81.2%), and the resulting biofouling was more severe than the control (68.3%). In marked contrast, the presence of 50 $mg \cdot L^{-1}$ NPs in ultrapure water only induced mild membrane fouling by the cake formation through particle precipitation. This indicated that the membrane biofouling caused by additive effects of NPs and microorganisms should be the main reason for the rapid flux decline, rather than the deposition of NPs particles solely.

It is well known that EPS deposition on membranes induces hydraulic resistance to permeation flux and elevated transmembrane osmotic pressure, leading to a decrease in membrane flux. The accumulation of EPS has various origins such as active secretion from microorganisms, cell lysis and sorption from environment (Shi et al., 2017). The content of the main biofouling components in the four typical filtration phases was quantified to further investigate how *P. aeruginosa* responded to NPs stress. As shown in Fig. 2b-c, the polysaccharide and protein contents increased considerably with the filtration time, which could explain the marked flux decline. In addition, the polysaccharide content in the biofilm was remarkably increased under the conditions of 0.1 and 1 $mg \cdot L^{-1}$ NPs, confirming that low NPs exposure promoted microbial polysaccharide secretion to form protective external layers. Promoting EPS formation is considered a defense response to reduce the damage of NPs to the intracellular environment, and enhance the adaptability of *P. aeruginosa* to the stresses caused by

NPs.

To further clarify the mechanisms involved, the viability of cells on the membrane surface exposed to NPs at different concentrations and contact times were determined (Fig. 2d). Consistent with the images shown in Fig. 1d, the bacterial activity was significantly inhibited at a NPs dosage of 50 $mg \cdot L^{-1}$. However, under 0.1 and 1 $mg \cdot L^{-1}$ NPs exposure, the ATP content increased compared with R0 (0 $mg \cdot L^{-1}$ NPs). This can be attributed to the following two aspects: (1) The promoted EPS secretion (especially polysaccharide) served as a protective barrier to reduce the NPs-induced stress and maintain bacterial viability; (2) the adhering EPS enhanced bacterial adhesion on the membrane surface.

The adhesion and biosynthesis of exopolysaccharides are crucial for cell-cell interactions, primary biofilm-related colonization and biofilm scaffold formation (Overhage et al., 2005). Alginate, Psl and Pel are the three main polysaccharides present in the EPS of *P. aeruginosa* strains, each of which associates with different biofilm development stages and providing specific physiological properties to the biofilm (Cendra and Torrents, 2021). In this study, we focused on three functional assignment genes (*algD*, *pslA*, and *pelA*), which are involved in the biosynthesis of alginate, Psl and Pel exopolysaccharide, respectively (Fig. 2e). The relative abundance of *algD* and *pelA* increased 1.27–1.69 and 1.20–1.37 fold under NPs exposure, compared with the control. As the initial gene in the *pel* gene cluster, *pelA* is essential for biofilm formation and the regulation of the entire *pel* operon in *P. aeruginosa* (Overhage et al., 2005). In comparison, the expression of *pslA* was suppressed by 14.7%–23.5% under NPs exposure, indicating a significant influence on the expression of polysaccharide secretion genes in *P. aeruginosa* (Fig. 2e).

The characterization of the membrane surface with and without fouling formation

provided more insights into the properties of foulant. In situ ATR-FTIR characterization (Fig. 2f) showed that, in the high-frequency region, a broad band at 3200–3400 cm^{-1} (H-bonds, OH groups) and a peak at 2940 cm^{-1} (antisymmetric stretching vibration peak of $-CH_3$) were detected. The peaks at 1654 cm^{-1} and 1550 cm^{-1} corresponded to the amide I band (mainly associated with the secondary structure of proteins) and the amide II band (reflecting the extent of proteins' adsorption), respectively, which define the characteristics of proteins (Jiang et al., 2022). In addition, three absorption bands were clearly observed at 1388, 1227 and 1045 cm^{-1}, corresponding to the bending vibration peak of -CHO, the stretching vibration peak of -O-C(O)-C and the C-O stretching of polysaccharides, respectively (Ivnitsky et al., 2005). Overall, the results revealed that all biofouled membranes accumulated an identical fingerprint profile, mainly composed of protein-like substances, as well as a high level of aliphatic and polysaccharide structures.

The relative elemental contents of the biofouled membranes were evaluated by XPS analysis, which showed that carbon (C), oxygen (O), nitrogen (N) and phosphorus (P) occupied a relatively high proportion in the biofouling layer (Fig. 2g). The total C content in the NPs-dosed biofilms (66.4%–71.3%) were greater than that of biofilms without NPs (63.1%), mainly due to the enrichment of NPs and enhanced EPS secretion (Table S5). The XPS spectra of the deconvoluted C1s peak were further analyzed (Fig. 2h), and the area percentages regarding the deconvoluted XPS C1s peaks of biofilms are shown in Table S6. The C1s peak was decomposed into four peaks with binding energies of 284.8, 286.4, 287.9 and 288.9 eV, respectively. The binding energies correspond to the following: 284.8 eV is mainly related to the C-H bond of the amino acid side chain and the aromatic ring (C-C/C=C); 286.4 eV represents the characteristic functional groups of C-O in ethers and alcohols or C-N in

amines and amides; 287.7 eV is related to carbonyl (C=O); 288.7 eV represents the ester or carboxyl group (O-C=O) (Magri et al., 2018; Wen et al., 2022; Xiong et al., 2022). Interestingly, the proportion of functional groups related to the amino acid side chain and aromatic ring (C-H/C-C/C=C) was 1.69 times that of the control group, for the 50 $mg \cdot L^{-1}$ NPs concentration. This can be attributed to two effects: (1) a high NPs-induced stress enhanced the release of bacterial intracellular organic matter; and (2) polystyrene NPs were enriched in the contaminated layer through membrane pore interception, EPS adhesion and self-agglomeration.

NPs particles were considered to be physically trapped in the biofilm matrix, thereby bonding to organic matter and exerting their effect on the biofilm. SEM images showed the distribution of NPs on the biofilm surface and cross-section area (Fig. 2i). A large number of NPs particles were captured in the rough surface regions, while others remained in the biofilm layer, indicating that EPS synthesis outside the biofilm cells induced aggregation of NPs particles. In addition, the pothole region on the surface of the filter could impede flow shear, hence facilitating the immobilization of NPs. Overall, two different states indicated that the change in water flow during filtration promoted the capture of NPs by adhesive EPS, as well as the aggregation of NPs on the membrane surface. In addition to the size exclusion effect of NF, the agglomeration of NPs and EPS adhesion also played important roles in NPs rejection.

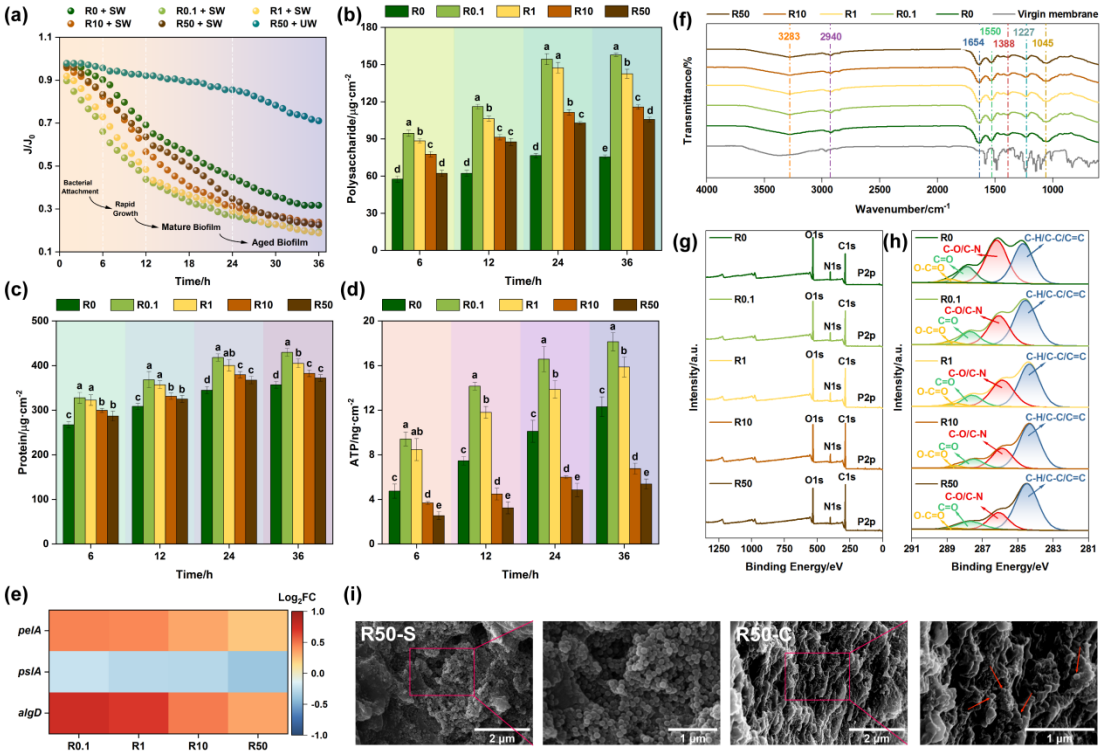


Fig. 2. Normalized water flux as a function of the fouling time exposure to increasing NPs concentrations (NPs: nanoplastics, SW: synthetic wastewater, UW: ultrapure water) (a); the content of polysaccharide (b), protein (c), and ATP (d) in biofouled layers; regulation of three polysaccharide biosynthesis genes (i.e., *pelA*, *pslA* and *algD*) following exposure to increasing concentrations of NPs after 12 h filtration; the quantification of each gene is expressed as the fold change (fold changes are $\log_2$ transformed) relative to the unexposed control (R0), and results are the mean of independent triplicates (e); in situ ATR-FTIR spectra (f), XPS spectra (g), and the deconvoluted C1s peak (h) of bio-contaminated membranes; SEM images of the surface (R50-S) and cross section (R50-C) of the membrane biofilm for 50 mg·L^{-1} NPs influent concentration (i).

3.3 NPs induced oxidative stress and enhanced cell membrane permeability

The responses of cells to NPs can be indicated by the changes in intracellular ROS and extracellular LDH, which represent the oxidative damage and mechanical damage to cell membranes, respectively (Zhai et al., 2024). A previous study reported that NPs could penetrate bacterial membranes and trigger ROS production under hydrophobic interactions and van der Waals forces (Liu et al., 2021). In our experiments, after 36 h

of dynamic filtration, the production of ROS was 1.29–1.76 times enhanced under NPs-induced stress (Fig. 3a). LDH is a peripheral membrane respiratory enzyme that is located on the cytoplasmic side of the inner membrane, and its function is to maintain a bacterial redox balance (Wang et al., 2021). Extracellular LDH levels significantly increased under high NPs-induced stress during the biofouling process, indicating that NPs increased the permeability of cell membrane through the combination of ROS generation and mechanical damage (Fig. 3b). The excessive accumulation of ROS destroyed membrane integrity, thus making the transfer of NPs across the cell membrane easier and causing a variety of cytotoxic effects.

As important scavengers of ROS, SOD (superoxide dismutase) and CAT (catalase) are essential defense against oxidative damage and to maintain redox equilibrium. Under normal circumstances, ROS, SOD and CAT form a dynamic balance to maintain the cellular homeostasis. SOD induces the dismutation of ROS into H_2O_2, while CAT further decomposes H_2O_2 into H_2O and O_2 (Gao et al., 2023). NPs greatly raised the SOD and CAT activity during the initial 24 h of filtration, indicating the occurrence of oxidative stress and antioxidant reaction. However, the sustained production of ROS exceeded the natural cleavage of antioxidant defense mechanisms over a long period of exposure time (36 h), as confirmed by the decreased SOD and CAT activities (Fig. 3c-d). The residual ROS can further induce lipid peroxidation, increase cell permeability and disrupt the microbial viability (Jia et al., 2023). Overall, the activity of antioxidant enzymes was enhanced to stimulate the defense system in response to NPs stress. With longer exposure time and higher exposure levels of NPs, the antioxidant defense system was disrupted and caused a certain degree of oxidative damage to the bacteria.

RDA (Fig. 3e) and PCA (Fig. 3f) were employed to comprehensively delineate the

relationships among the properties of biofouled membranes. The ATP content was highly negatively correlated with NPs concentration, mainly due to severe cell damage under NPs-induced stress. In addition, the content of protein showed a more negative response to the normalized flux, compared with polysaccharide, due to its hydrophobicity and higher content in biofilms. However, the negative correlation between NPs concentrations and polysaccharide was more significant compared with protein, consistent with the previous discussion of the results in Fig. 2b. Based on the staining and confocal images obtained from the fluorescence microscope, there are observable differences between the biofouled NF membranes with and without NPs (Fig. 3g). The dead cell percentage increased 24.1%–37.2% under higher NPs exposure, compared with the control. Consistent with the analysis of SEM images, filtering of the blue fluorescent NPs (1 mg·L^{-1}) in the NF systems illustrated that the fluorescent NPs were agglomerated and uniformly distributed on the membrane surface (R1-F).

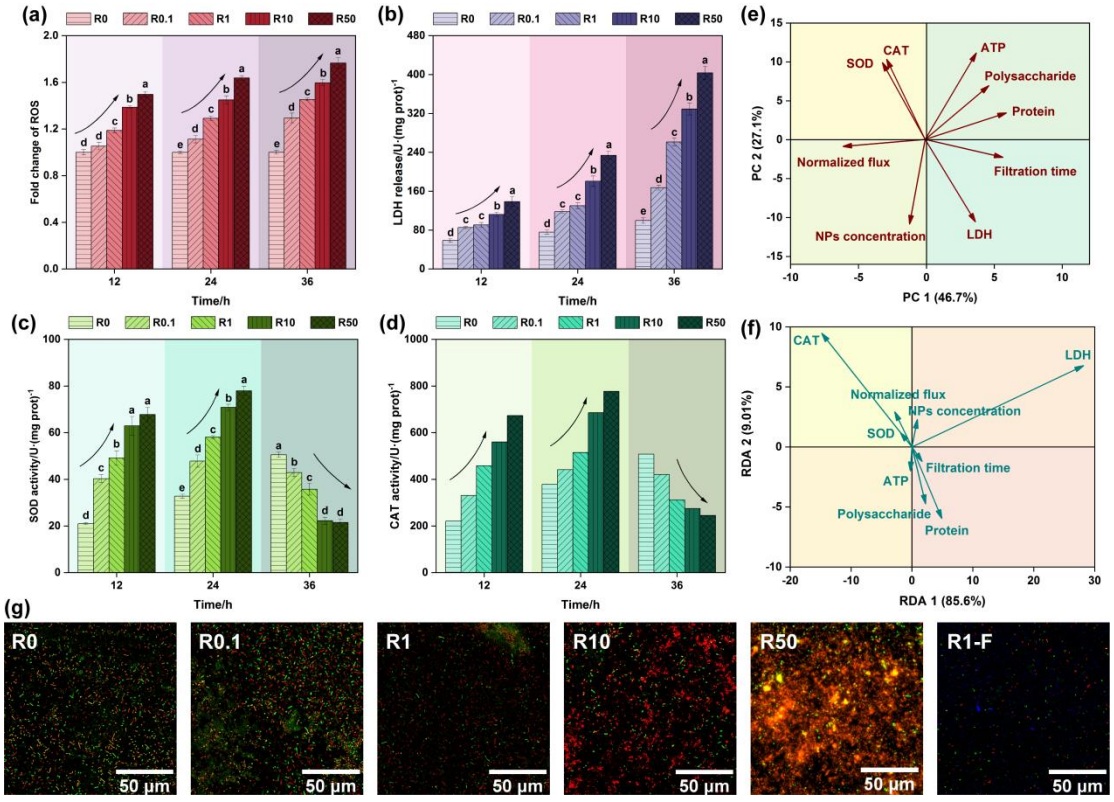


Fig. 3. Fold changes of ROS production (a), SOD (c), and CAT activities (d) of bacteria in the biofouling layers; released LDH levels (b) of biofilm extraction supernatants; principal component analysis (e) and redundancy analysis (f) of the test parameters in the dynamic biofouling process; CLSM images of live and dead cells of the biofilms (g).

3.4 Transcriptome analysis and the homologous recombination pathway

To characterize the transcriptional changes in the physiology of *P. aeruginosa* in membrane biofilms, we compared the transcriptomes with (0.1 and 50 $mg \cdot L^{-1}$) and without (0 $mg \cdot L^{-1}$) NPs stress, particularly R0.1 vs. R0 and R50 vs. R0. Biofilms were sampled at the initial stage of mature biofilm formation (12 h) to reduce the RNA degradation. We identified 431 and 518 significantly differentially expressed genes when comparing R0 vs. R0.1 and R0 vs. R50 ($|\log_2 FC| > 1$, $p < 0.05$), respectively, of which 287 differentially expressed genes were similar in both comparisons (Fig. 4a-b). Oxidative stress caused by NPs was observed in the changed expression genes related to ROS production (*dsbA* and *PA0846*), which were 1.23–1.76 times upregulated after NPs exposure. According to the previous discussion, the catalase and superoxide dismutase activities of the *P. aeruginosa* strain increased under NPs exposure due to excessive ROS interaction. Correspondingly, the highly expressed antioxidant genes (i.e., *sodB*, *sodM*, *katA* and *katB*) might be necessary for resistance to ROS stress (Fig. 4d). In addition, the *ahpC* gene related to antioxidant activity was 1.25–1.43 times upregulated under NPs stress, which facilitated alkyl hydroperoxide reductase encoding and the reduction of hydroperoxide catalyzing to reduce oxygen radical damage. Another gene related to antioxidant defense systems (i.e., *trxA* for thioredoxin) was also over expressed (1.45–1.76 fold), indicating that the NPs-induced ROS stress increased the cellular defensive ability.

A recent study found that thermal stress upregulated genes encoding

endonuclease, mismatch repair protein, and exodeoxyribonuclease to repair DNA damage, resulting in an enhanced role in SOS response and DNA repair pathways (Ren et al., 2022). Considering that ROS could chemically modify and oxidize macromolecules (e.g., DNA, RNA, and proteins), exposed DNA is susceptible to permanent oxidative damage, and DNA repair became essential for survival. Here, we noticed the expressions of related genes in DNA polymerase III subunits (*dnaE*, *dnaX* and *dnaQ*), holliday junction ATP-dependent DNA helicase (*ruvA* and *ruvB*), crossover junction endodeoxyribonuclease (*ruvC*) and recombination protein (*recA*, *recB* and *recR*) inside *P. aeruginosa* displayed an upregulation, which were essential for the accurate repair of DNA double-strand breaks (Fig. 4c-d). As a result of higher NPs exposure (R50), the primosome assembly gene *priA*, DNA polymerase III subunit gene *dnaN*, exodeoxyribonuclease V subunit gene *recD*, and DNA repair gene *recO* and *recN* were downregulated, mainly due to the NPs-induced direct DNA damage inside cells. Therefore, as a result of exposure to NPs, DNA repair and primosome assembly were activated to resist the corresponding stress response. However, the severe disruption of DNA caused by NPs-induced ROS may hamper functional gene expression and lead to the death of bacteria.

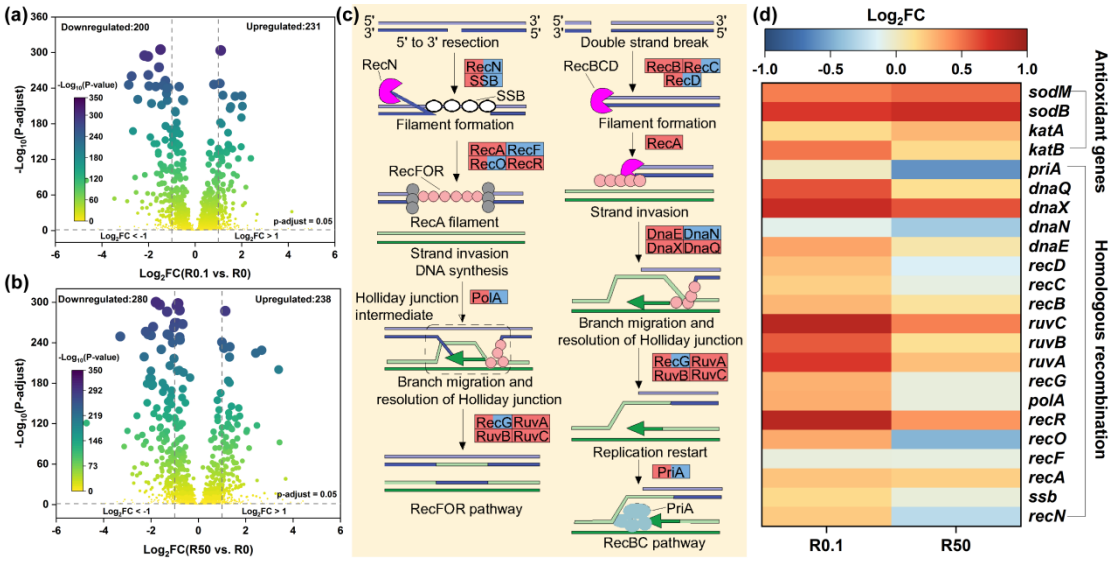


Fig. 4. Volcano plot showing the differential gene expression shared between R0.1 vs. R0 (a) and R50 vs. R0 (b) comparisons, with schematic representation of the homologous recombination of *P. aeruginosa* exposed to NPs; the downregulation (blue squares) and upregulation (red squares) of proteins/genes, with R0.1 vs. R0 on the left and R50 vs. R0 on the right (c), the meanings of these symbols are the same below; transcriptional expression of genes responsible for oxidative stress and homologous recombination (d).

3.5 Extracellular polysaccharides biosynthesis and bacterial secretion system

Bacterial EPS synthesis enhances survivability in adverse and extreme environments, which further results in aggregated biofilm formation (Yu et al., 2023). Understanding the genetic regulation and biosynthetic pathways of exopolysaccharides and bacterial secretion systems is crucial for understanding the structure and stability of biofilm. The exopolysaccharides of the EPS, namely alginate, Pel and Psl production, are an integral part of the biofilm matrix. The assorted *alg*, *pel* and *psl* genes involved in exopolysaccharides biosynthesis are shown in Fig. 5a, each of which plays a distinctive role in biofilm formation. Alginate is a linear heteropolysaccharide with an anionic nature, which is necessary for water and nutrient retention in biofilms (Ma et al., 2022). Pel is positively charged and promotes cell-cell interaction, adhesion, aggregation and protection. Psl is a neutral pentasaccharide repeat unit of D-mannose, D-glucose and L-rhamnose, which not only helps in providing resistance and maintaining biofilm structure, but also acts as a signal molecule to regulate exopolysaccharide production and biofilm formation (Vandana and Das, 2022). The transcription of *alg* and *pel* operon were activated under low concentrations of NPs exposure (Fig. 5c). In comparison, the expression of the *psl* gene cluster showed opposite effect, with it being downregulated at both low and high NPs concentrations. Therefore, the overproduction of Pel and alginate contributed to higher polysaccharide contents

under NPs exposure, while the production of Psl was suppressed with increasing NPs exposure. The accuracy of transcriptomics results was consistent with RT-qPCR analysis, with a correlation coefficient (R^2) up to 0.92 (Fig. S4).

The protein component stabilizes the biofilm matrix and develops a three-dimensional architecture through interaction with extracellular polysaccharides (Yu et al., 2023). The production of extracellular proteins is a highly regulated process controlled by a cascade of interconnected regulatory networks (Fig. 5b). *P. aeruginosa* T2SS is a two-step secretion system in which substrates are exported into the periplasm using the Sec-/Tat- pathway firstly, and then across the outer-membrane through a dedicated channel (Pourhassan et al., 2021). In addition, bacteria living in adverse environments can secrete hydrolytic enzymes that function as nutrient acquisition using T2SS (Weng et al., 2022). The T3SS is a highly conserved virulence structure that plays an important role in bacterial pathogenicity, which forms needle-like machines on the bacterial surface to inject effector proteins into host cells (Hauser, 2009). The T6SS injects toxins (e.g., peptidoglycan hydrolases) into competing bacteria, which links to biofilm formation processes by co-regulating with the *psl* and *pel* loci (Hood et al., 2010). The upregulated expression of outer and inner membrane proteins biosynthesis in R0.1 indicates that the cell membrane was stressed by low NPs levels, which enhanced the biosynthesis and modification of extracellular proteins to prevent NPs from entering cells and to alleviate the damage to the cell (Fig. 5d). With higher NPs exposure, the expression of genes encoding type II secretion system proteins (*xcpP*, *xcpY* and *xcpR*), type III secretion system proteins (*pscF*, *pscC*, *pscP*, *pscR*, *pscQ* and *PA1692*) and fha domain-containing protein (*fha1*) were highly dounregulated. Therefore, biofilms formed in R50 that express deficient bacterial secretion systems may exhibit an unstable biofilm matrix, considering the suppressed

functional bacterial secretion gene expression (especially in T3SS).

Previous research has suggested that NPs could increase membrane permeability by inducing surface reconstruction of cell membrane (Wang et al., 2008). The outer membrane of *P. aeruginosa* is a selective permeation barrier, which allows uptake of nutrients while simultaneously protecting the bacteria from harmful compounds (Grimm et al., 2020). The reduction of outer membrane proteins (OMPs) can weaken the outer membrane, alter cell shape and lead to outer membrane rupture (Mikheyeva et al., 2023). In this study, two key genes encoding OMPs biosynthesis (i.e., *popN* and *PA1666*) were downregulated in R50, which eventually caused the membrane integrity damage. In addition, three genes (i.e., *waaP*, *PA1386* and *PA4460*) encoding the biosynthesis of lipopolysaccharide, the integral component of cell membrane, were also highly suppressed in R50. Overall, our results show that low and high NPs exposure regulated the bacterial metabolic pathway of EPS production in different ways in response to changes in environmental conditions. The involvement of extracellular polysaccharides and proteins in membrane biofilms potentiates their roles in NPs biosorption and complex formation.

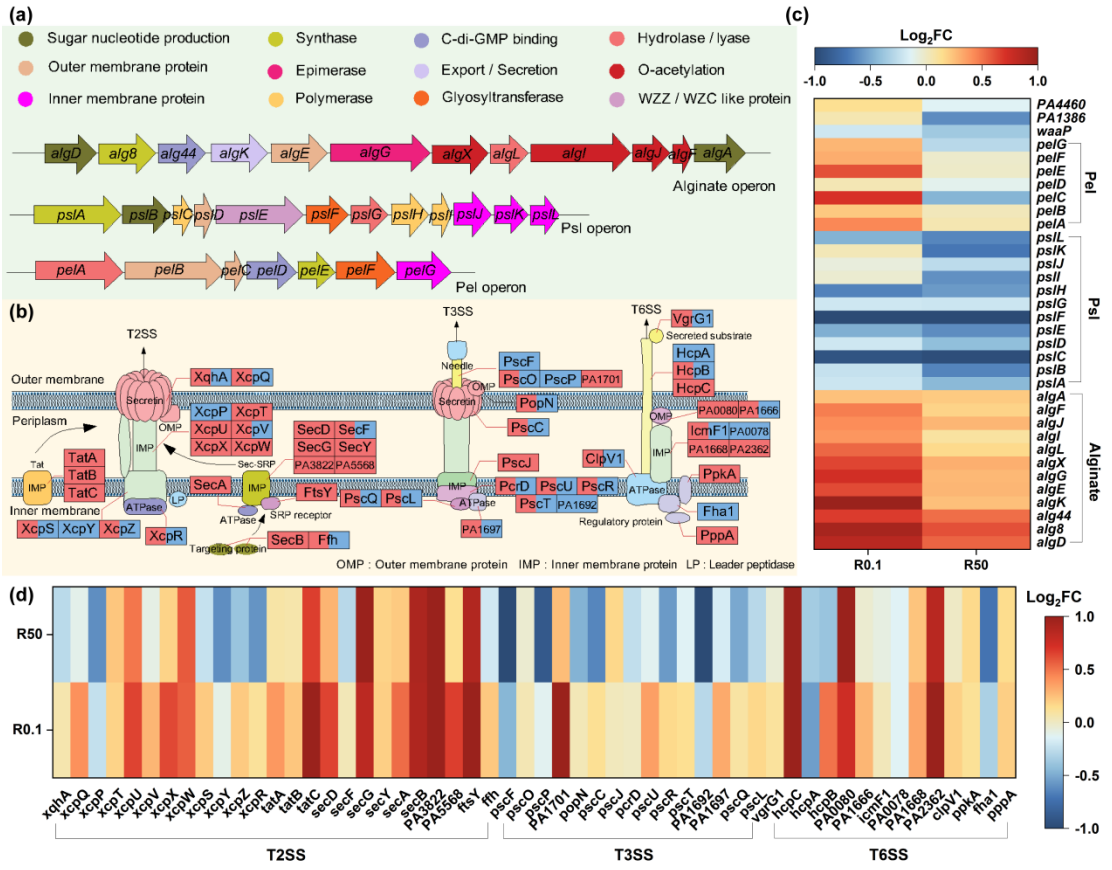


Fig. 5. Gene clusters and regulations of exopolysaccharides in *P. aeruginosa*, genes were categorized according to their putative functions and indicated with colored arrows (a); schematic representation of the protein export via different bacterial secretion systems (i.e., T2SS, T3SS, and T6SS) of *P. aeruginosa* exposed to NPs (b); transcriptional expression of genes responsible for extracellular polysaccharide biosynthesis (c) and bacterial secretion system (d).

3.6 Quorum sensing and virulence factor production

Quorum sensing (QS) is a bacterial communication process that controls bacterial biofilm formation and virulence regulation by sharing information about cell density and adjusting gene expression accordingly (Bodelon et al., 2016). As shown in Fig. 6a, the effects of influent NPs concentrations on the QS pathway showed a non-unidirectional trend, with high concentration inhibition and low concentration promotion. The expression levels of gene coding for hypothetical protein (*PA2569*), riboflavin-specific deaminase/reductase (*ribD*), inner membrane protein translocase

589 (*PA5568*), pyridoxamine 5'-phosphate oxidase (*phzG1*), phenazine biosynthesis
590 protein (*phzD1* and *phzD2*) and trans-2,3-dihydro-3-hydroxyanthranilate isomerase
591 (*phzF2*) were highly elevated in R0.1 as compared to R0. However, the expression
592 levels of genes coding for acyl homoserine lactones (AHLs) QS transcription factors
593 (*lasR* and *rhlR*), anthranilate synthase component (*phnA* and *phnB*) and phenazine
594 biosynthesis protein (*phzB1*, *phzB2* and *phzG2*) were supressed in R50 (Fig. 6b). *P.*
595 *aeruginosa* has four QS signaling systems (i.e., LasR/I, RhlR/I, PQS, and IQS). As a
596 hierarchical network, LasI/R is located at the top of the QS system, regulating other QS
597 genes such as *rhlI/R* and *pqsA/B/C/D/E* (Whiteley et al., 2018). As the most common
598 QS signaling molecules in *P. aeruginosa*, AHLs bind to the receptor leading to the
599 repression or activation of target genes (Fig. 6c). Two genes that encode soluble lectins
600 (*lecA* and *lecB*), important virulence factors in *P. aeruginosa*, were also slightly
601 upregulated in R0.1. Both LecA and LecB contribute to biofilm formation by
602 cross-linking with bacterial polysaccharides (e.g., lipopolysaccharide and mannose),
603 which enhances bacterial retention and aggregation (Cendra and Torrents, 2021).

604 The formation and stability of biofilms are also highly dependent on rhamnolipid
605 biosynthesis (RB) and phenazine biosynthesis (PB), where rhamnolipid facilitates the
606 biofilm establishment and maintenance by facilitating the availability of nutrients and
607 oxygen, and phenazine supports metabolic activity in hypoxic/anoxic biofilm subzones
608 (Evans et al., 2023; Feng et al., 2021). The gene expression of anthranilate synthase
609 (*phnA* and *phnB*), which is responsible for proteoglycan and glycoprotein production
610 by inducing anthranilate and its derivative formation, was upregulated in R0.1.
611 Previous research found that cells inside the biofilm matrix communicate via
612 self-produced QS molecules that regulate extracellular polysaccharide production (Lee
613 et al., 2023). For instance, LasR binds with the promoter of the *psl* operon and regulates

psl expression, while the *rhl* system facilitates Pel and rhamnolipid biosynthesis. The repressed QS expression in R50 further reduced the biosynthesis of virulence factors (e.g., lectin, phenazine and rhamnolipid). Consistent with QS pathway regulations, the expression of rhamnolipid and phenazine biosynthesis-associated genes was also upregulated in R0.1, thereby enhancing bacterial resistance to NPs by promoting biofilm formation.

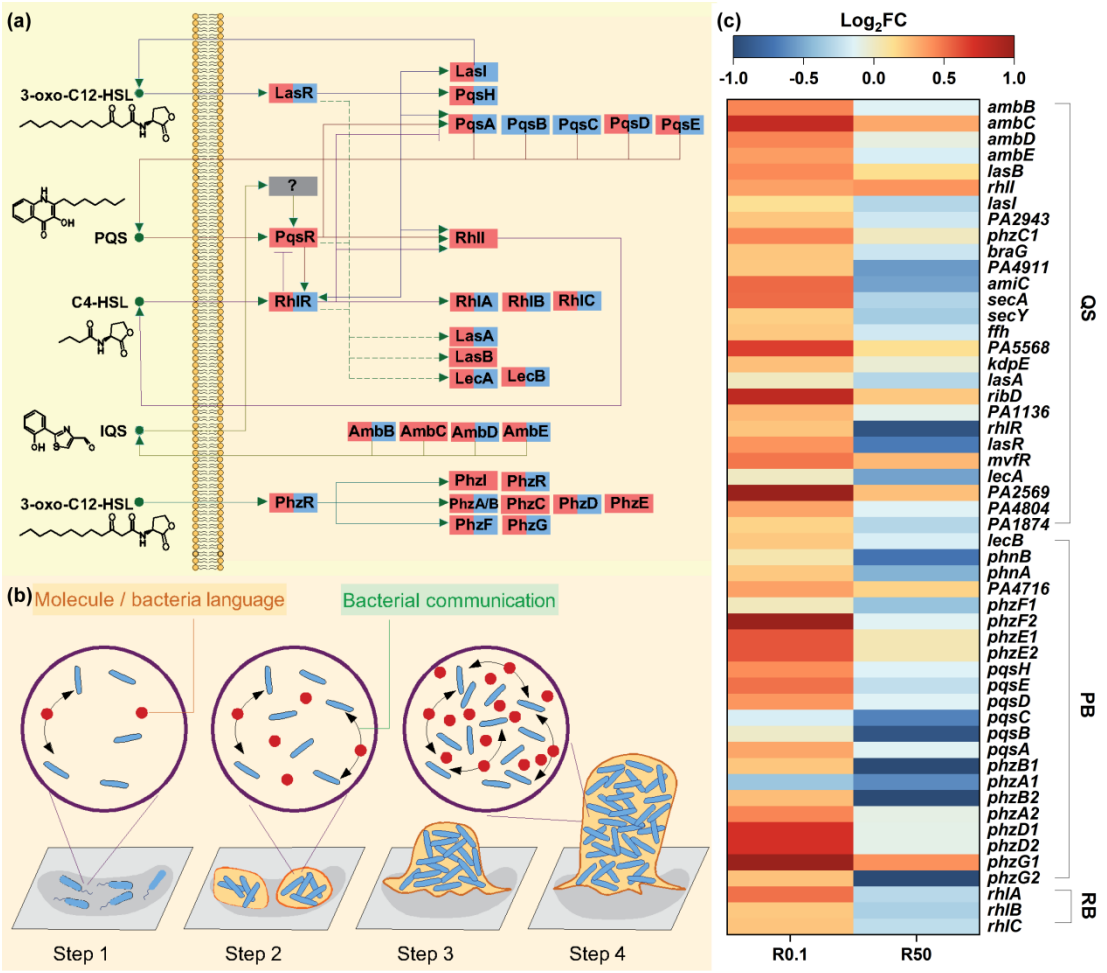


Fig. 6. Schematic representation of the four QS signaling systems (LasR/I, RhlR/I, PQS, and IQS) in *P. aeruginosa*, and their interaction with colored lines; arrows indicate a stimulatory effect, while perpendicular lines indicate an inhibitory effect; the solid lines indicate a direct interaction, while the dashed lines indicate an indirect interaction (a); transcriptional expression of genes responsible for quorum sensing (QS), rhamnolipid biosynthesis (RB) and phenazine biosynthesis (PB) in *P. aeruginosa* exposed to NPs (b); diagram showing the four *P. aeruginosa* biofilm maturation processes (i.e., initial attachment, cell-cell adhesion, microcolony formation and the maturation

phase), and the expression of bacterial QS molecules which varies according to community density (c).

3.7 Glycolysis/gluconeogenesis and tricarboxylic acid cycle

Energy metabolism plays an important role in biological anabolism (e.g., the synthesis of fatty acids, carbohydrates, and amino acids), the metabolic process and physiological behavior. The glycolysis/gluconeogenesis and tricarboxylic acid cycle (TCA cycle) are two vital pathways that provide energy and crucial metabolic precursors for various key metabolic pathways, which may be seriously affected by NPs stress. The genes associated with different steps of the glycolysis/gluconeogenesis and TCA cycles were annotated, and we found the concentration-dependence of expressed genes in *P. aeruginosa* after NPs treatment. Multiple enzymes involved in glycolysis/gluconeogenesis (Fig. 7a) and the TCA cycle (Fig. 7b) were upregulated in R0.1 and downregulated at R50, which further supported the idea that NPs regulate energy metabolism differently with changed exposure concentrations.

Genes that encode key enzymes of substrate level phosphorylation, such as glyceraldehyde-3-phosphate dehydrogenase (NADP+) [EC:1.2.1.9] and pyruvate kinase [EC:2.7.1.40], were upregulated 1.41-fold and 1.93-fold in R0.1, respectively, which promoted energy production (ATP and NADH) for cell growth (Liu et al., 2024). Genes encoding the rate-limiting enzyme pyruvate carboxylase [EC:6.4.1.1] and several critical enzymes like aconitate hydratase [EC:4.2.1.3], fumarate hydratase [EC:4.2.1.2], succinate dehydrogenase (ubiquinone) flavoprotein subunit [EC:1.3.5.1], isocitrate dehydrogenase [EC:1.1.1.42] and the 2-oxoglutarate dehydrogenase E1 component [EC:1.2.4.2] in the TCA cycle were also upregulated in R0.1. In addition, the expression level of genes corresponding to phosphoenolpyruvate carboxykinase (*pckA*), pyruvate carboxylase subunit (*PA5435*), acetyl-CoA carboxylase subunit

(*PA5436*) and succinate dehydrogenase subunits (*sdhA*, *sdhC* and *sdhD*) were highly upregulated in R0.1 (Fig. 7c). The upregulation of genes related to the TCA cycle in R0.1 provide more essential precursors (e.g., ATP, NADH, amino acids, and acetyl-CoA) for other metabolic pathways, which enhances the carbon metabolism process to provide more energy and materials for bacterial vitality. A previous study also demonstrated that molybdenum disulfide nanoparticles (50 $\mu g \cdot L^{-1}$) could stimulate glycolytic flux (Luo et al., 2022). In comparison, a general inhibition of both pathways was observed in R50, indicating that high NPs-induced stress could disrupt microbial energy metabolism and biological anabolism.

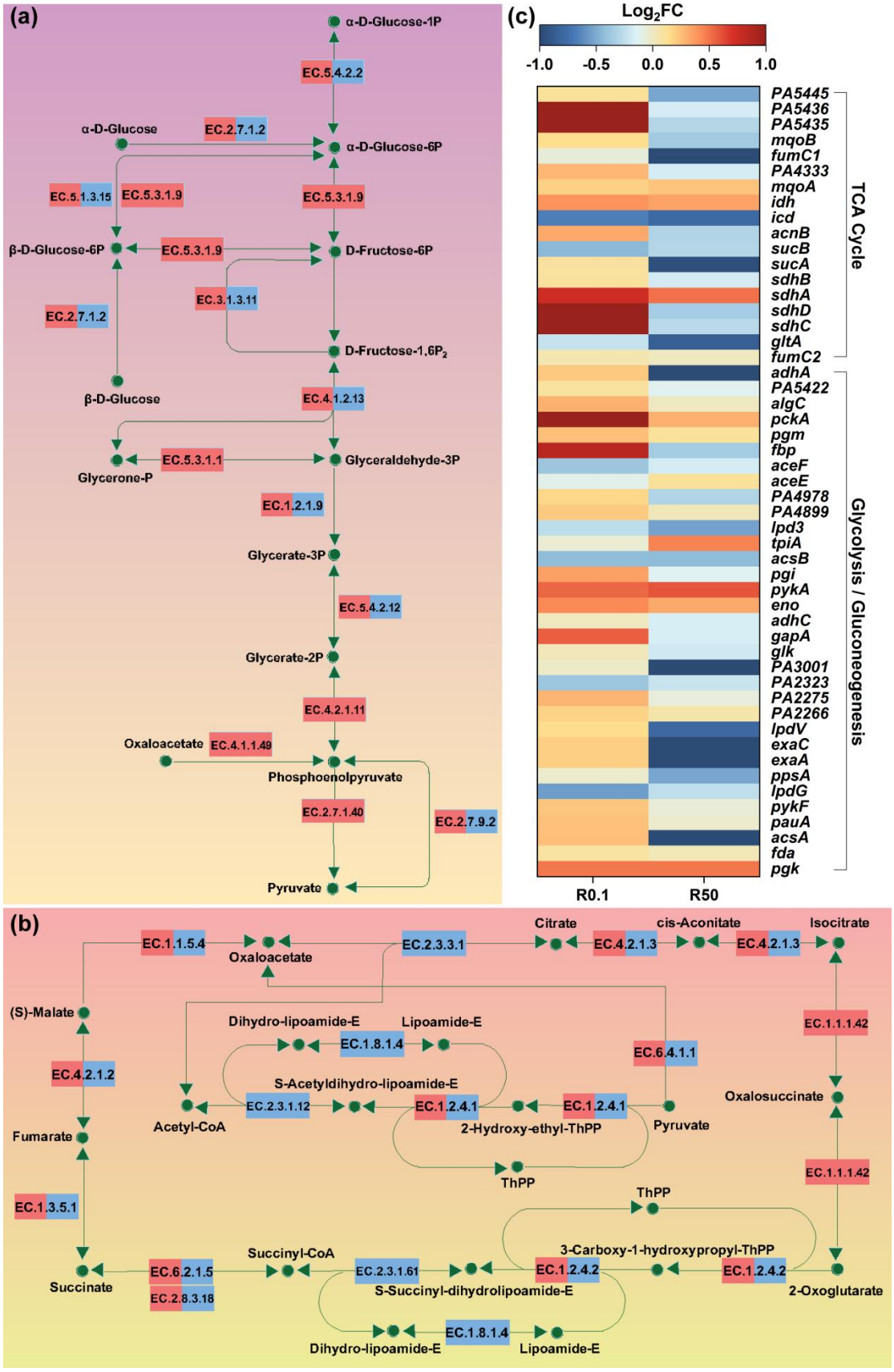


Fig. 7. KEGG glycolysis/gluconeogenesis (a) and tricarboxylic acid cycle (TCA cycle) (b) diagrams of *P. aeruginosa* after exposure to 0.1 mg·L^{-1} (R0.1) and 50 mg·L^{-1} (R50) NPs; transcriptional

666 expression of genes responsible for the glycolysis/gluconeogenesis and TCA cycles in *P.*
667 *aeruginosa* exposed to NPs (c).
668
669 **3.8 Oxidative phosphorylation and flagellar assembly**
670 Oxidative phosphorylation is an intracellular biochemical process that utilizes the
671 energy generated by the proton gradient driven by complex V to convert ADP to ATP
672 (Fig. 8a). The produced ATP can be used for maintaining metabolic processes under
673 NPs-induced stressful condition (Ren et al., 2022). The *nuo* operon encodes the NADH
674 ubiquinone oxidoreductase, which couples the transferred electrons from NADH to
675 ubiquinone with protons translocation at the cytoplasmic membrane (Weng et al., 2022).
676 The expression of several genes (e.g., quinone oxidoreductase of
677 *nuoA/B/D/E/F/G/H/I/J/L/N*) related to transmembrane protein complex I was
678 downregulated in R50, suggesting high NPs exposure slowed down the respiration of *P.*
679 *aeruginosa*. Similarly, the gene expression related to ATP synthase for complex V (e.g.,
680 F-type ATPase of *atpA/D/E/G/H*) was also highly downregulated under high NPs stress
681 (Fig. 8c). The suppressed oxidative phosphorylation at R50 decreased electron supply,
682 weakened proton transmembrane and eventually inhibited microbial energy production
683 and metabolism.
684 Cell motility is an energy-demanding process that is a behavioral adaptive
685 response that enables cells to escape from harsh environments (Zhang et al., 2020b). In
686 *P. aeruginosa*, flagella contribute to bacterial adhesion and colony formation. A slight
687 upregulation of genes in the flagellar assembly pathway was observed in R0.1, which is
688 considered a defensive strategy used by bacteria to form biofilms. In addition, some
689 bacteria are released from mature membrane biofilms, and higher cell motility can
690 trigger the released cells to search for favorable environments and better access to local
691 nutrients in the biofilms (Yu et al., 2023). In contrast to previous swarming ability tests

(Fig. 1c), the expression of genes related to MS/C/D/L ring, distal rod and hook assembly was downregulated in R50, which was mainly attributed to different bacteria lifestyles (i.e., free-living cells vs. sessile communities) and the reduced ATP synthesis (Fig. 8b). Several genes function in the C ring (*fliG/M/N*), which are responsible for both torque generation and switching the direction of motor rotation, were 0.54- to 0.88-fold downregulated in R50 (Zhang et al., 2019). These results indicate that changes in flagella-mediated mobility are another important type of behavior-based plasticity in response to NPs-induced stress.

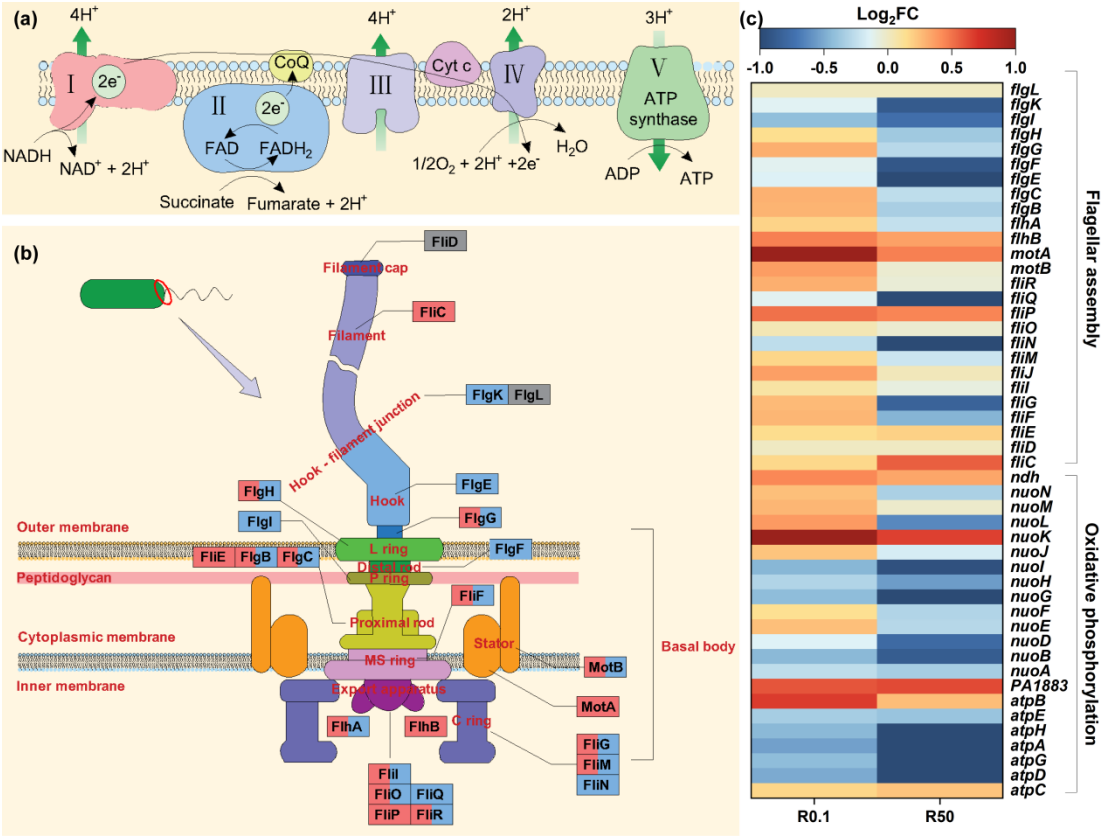


Fig. 8. Schematic representation of the oxidative phosphorylation (a) and flagellar assembly (b) of *P. aeruginosa* exposed to NPs; the colored square represents the downregulation (blue), upregulation (red) and no change (gray) of proteins/genes, with R0.1 vs. R0 on the left and R50 vs. R0 on the right; transcriptional expression of genes responsible for flagellar assembly and oxidative phosphorylation in *P. aeruginosa* exposed to NPs (c).

4. Conclusions

In this study, for the first time, the interaction between the dynamic membrane biofouling stages stimulated by bacterial attachment (0–6 h), rapid growth (6–12 h), maturation (12–24 h), aged biofilm (24–36 h) and increasing NPs concentrations (0–50 $mg \cdot L^{-1}$) have been explored. The results indicated a functional regulation of bacteria adaptation to NPs stress, which further exhibited significant effects on biofouling behaviors in the NF system. A low NPs condition (0.1 $mg \cdot L^{-1}$) promoted extracellular polysaccharide biosynthesis and biofilm formation by stimulating the QS process, energy metabolism and bacterial secretion systems, while a high NPs exposure (50 $mg \cdot L^{-1}$) induced metabolic inactivation, cell lysis and the release of intracellular matter due to triggered ROS generation, genomic DNA damage and a shortage of ATP. Overall, these self-regulations protected bacteria from NPs-induced stress and enhanced their ability to adapt, at the cost of changes in matter and energy metabolic pathways. Since low concentrations of NPs are typically found in WWTPs, more attention should be paid to the promoting effect of NPs on membrane biofouling behavior in WWTPs.

5. Future implications

As the global consumption of plastic products increases, a large amount of NPs particles pass into the aquatic environment and are further rejected by membrane filtration processes in water/wastewater treatment systems. Excessive NPs loading can trigger serious membrane biofouling formation and other negative environmental consequences. The observed upregulation of virulence-related genes in biofilms has suggests the potential for exacerbating bacterial pathogenesis and posing a risk to public health, which underscores the necessity of controlling the presence of high levels of NPs. Consequently, subsequent studies concerning the coupling effects of interfering ions and natural organic compounds could provide valuable new

information about the role of NPs on bacterial metabolic function under different intake conditions. The findings of this study provide an important perspective on the toxicological significance of NPs and a greater understanding of the potential risks to the performance of NF technology in full-scale water/wastewater treatment.

Acknowledgments

This work was supported by National Natural Science Foundation of China (Grant No. 52070018) and National Key Research and Development Program of China (Grant No. 2021YFC3201403).

References

Ban, Y., Tan, J., Xiong, Y., Mo, X., Jiang, Y. and Xu, Z. 2023. Transcriptome analysis reveals the molecular mechanisms of *Phragmites australis* tolerance to CuO-nanoparticles and/or flood stress induced by arbuscular mycorrhizal fungi. Journal of Hazardous Materials 442.

Bereschenko, L.A., Stams, A.J.M., Euverink, G.J.W. and van Loosdrecht, M.C.M. 2010. Biofilm formation on reverse osmosis membranes is initiated and dominated by *Sphingomonas* spp. Applied and Environmental Microbiology 76(8), 2623-2632.

Bodelon, G., Montes-Garcia, V., Lopez-Puente, V., Hill, E.H., Hamon, C., Sanz-Ortiz, M.N., Rodal-Cedeira, S., Costas, C., Celiksoy, S., Perez-Juste, I., Scarabelli, L., La Porta, A., Perez-Juste, J., Pastoriza-Santos, I. and Liz-Marzan, L.M. 2016. Detection and imaging of quorum sensing in *Pseudomonas aeruginosa* biofilm communities by surface-enhanced resonance Raman scattering. Nature Materials 15(11), 1203-1211.

Cendra, M.D. and Torrents, E. 2021. Pseudomonas aeruginosa biofilms and their partners in crime. Biotechnology Advances 49, 15.

Cui, L., Chen, P., Zhang, B., Zhang, D., Li, J., Martin, F.L. and Zhang, K. 2015. Interrogating chemical variation via layer-by-layer SERS during biofouling and cleaning of nanofiltration membranes with further investigations into cleaning efficiency. Water Res. 87, 282-291.

Enfrin, M., Lee, J., Fane, A.G. and Dumee, L.F. 2021. Mitigation of membrane particulate fouling by nano/microplastics via physical cleaning strategies. Science of the Total Environment 788.

Evans, C.R., Smiley, M.K., Asahara Thio, S., Wei, M., Florek, L.C., Dayton, H., Price-Whelan, A., Min, W. and Dietrich, L.E.P. 2023. Spatial heterogeneity in biofilm metabolism elicited by local control of phenazine methylation. Proceedings of the National Academy of Sciences of the United States of America 120(43), e2313208120-e2313208120.

Feng, Q., Luo, L., Chen, X., Zhang, K., Fang, F., Xue, Z., Li, C., Cao, J. and Luo, J. 2021. Facilitating biofilm formation of *Pseudomonas aeruginosa* via exogenous N-Acy-L-homoserine lactones

stimulation: Regulation on the bacterial motility, adhesive ability and metabolic activity. Bioresource Technology 341.

Gao, D.D., Kong, C.M., Liao, H.P., Junaid, M., Pan, T., Chen, X.K., Wang, Q.P., Wang, X. and Wang, J. 2023. Interactive effects of polystyrene nanoplastics and 6:2 chlorinated polyfluorinated ether sulfonates on the histomorphology, oxidative stress and gut microbiota in Hainan Medaka (*Oryzias curvinotus*). Science of the Total Environment 880, 12.

Grimm, J., Shi, H.D., Wang, W., Mitchell, A.M., Wingreen, N.S., Huang, K.C. and Silhavy, T.J. 2020. The inner membrane protein YhdP modulates the rate of anterograde phospholipid flow in *Escherichia coli*. Proceedings of the National Academy of Sciences of the United States of America 117(43), 26907-26914.

Hauser, A.R. 2009. The type III secretion system of *Pseudomonas aeruginosa*: infection by injection. Nature Reviews Microbiology 7(9), 654-665.

Heffernan, R., Semiao, A.J.C., Desmond, P., Cao, H., Safari, A., Habimana, O. and Casey, E. 2013. Disinfection of a polyamide nanofiltration membrane using ethanol. Journal of Membrane Science 448, 170-179.

Hood, R.D., Singh, P., Hsu, F., Guevener, T., Carl, M.A., Trinidad, R.R.S., Silverman, J.M., Ohlson, B.B., Hicks, K.G., Plemel, R.L., Li, M., Schwarz, S., Wang, W.Y., Merz, A.J., Goodlett, D.R. and Mougous, J.D. 2010. A type VI secretion system of *Pseudomonas aeruginosa* targets, a toxin to bacteria. Cell Host & Microbe 7(1), 25-37.

Horton, A.A., Walton, A., Spurgeon, D.J., Lahive, E. and Svendsen, C. 2017. Microplastics in freshwater and terrestrial environments: Evaluating the current understanding to identify the knowledge gaps and future research priorities. Science of the Total Environment 586, 127-141.

Hu, Y., Kang, Y., Huang, F., Su, Y., Zhou, X., Wang, A.-J. and Gao, S.-H. 2022. Distinct responses of *Pseudomonas aeruginosa* PAO1 exposed to different levels of polystyrene nanoplastics. Science of the Total Environment 852.

Ivnitsky, H., Katz, I., Minz, D., Shimoni, E., Chen, Y., Tarchitzky, J., Semiat, R. and Dosoretz, C.G. 2005. Characterization of membrane biofouling in nanofiltration processes of wastewater treatment. Desalination 185(1-3), 255-268.

Jafari, M., D'Haese, A., Zlopasa, J., Cornelissen, E.R., Vrouwenvelder, J.S., Verbeken, K., Verliefde, A., van Loosdrecht, M.C.M. and Picioreanu, C. 2020. A comparison between chemical cleaning efficiency in lab -scale and full-scale reverse osmosis membranes: Role of extracellular polymeric substances (EPS). Journal of Membrane Science 609.

Jia, H.W., Yu, H.W., Li, J.W., Qi, J., Zhu, Z.Q. and Hu, C.Z. 2023. Trade-off of abiotic stress response in floating macrophytes as affected by nanoplastic enrichment. Journal of Hazardous Materials 451, 14.

Jiang, T., Tian, T., Guan, Y.-F. and Yu, H.-Q. 2022. Contrasting behaviors of pre-ozonation on ceramic membrane biofouling: Early stage vs late stage. Water Res. 220.

Lee, K., Park, Y.-J., Iqbal, T., Park, H., Jung, Y., Shin, J.-H. and Choo, K.-H. 2023. Does quorum quenching matter to microbial community dynamics in long-term membrane bioreactor operation? Water Res. 244.

Liu, C.C., Zhu, X.Y., You, L.H., Gin, K.Y.H., Chen, H. and Chen, B.L. 2023. Per/polyfluoroalkyl substances modulate plasmid transfer of antibiotic resistance genes: A balance between oxidative stress and energy support. Water Res. 240, 11.

Liu, L., Xu, K., Zhang, B., Ye, Y., Zhang, Q. and Jiang, W. 2021. Cellular internalization and release of polystyrene microplastics and nanoplastics. Science of the Total Environment 779.

Liu, M., Zhang, L., Yang, R., Cui, H., Li, Y., Li, X. and Huang, H. 2024. Integrating metal-organic framework ZIF-8 with green modifier empowered bacteria with improved bioremediation. Journal of hazardous materials 461, 132475-132475.

Luo, L.-W., Wu, Y.-H., Chen, G.-Q., Wang, H.-B., Wang, Y.-H., Tong, X., Bai, Y., Xu, Y.-Q., Zhang, Z.-W., Ikuno, N. and Hu, H.-Y. 2022. Chlorine-resistant bacteria (CRB) in the reverse osmosis system for wastewater reclamation: Isolation, identification and membrane fouling mechanisms. Water Res. 209.

Ma, L.Z., Wang, D., Liu, Y., Zhang, Z. and Wozniak, D.J. 2022. Regulation of biofilm exopolysaccharide biosynthesis and degradation in *Pseudomonas aeruginosa*. Annual Review of Microbiology 76, 413-433.

Magri, D., Sanchez-Moreno, P., Caputo, G., Gatto, F., Veronesi, M., Bardi, G., Catelani, T., Guarnieri, D., Athanassiou, A., Pompa, P.P. and Fragouli, D. 2018. Laser ablation as a versatile tool to mimic polyethylene terephthalate nanoplastic pollutants: Characterization and toxicology assessment. Acs Nano 12(8), 7690-7700.

Malankowska, M., Echaide-Gorriz, C. and Coronas, J. 2021. Microplastics in marine environment: a review on sources, classification, and potential remediation by membrane technology. Environ. Sci.-Wat. Res. Technol. 7(2), 243-258.

Mikheyeva, I.V., Sun, J.W., Huang, K.C. and Silhavy, T.J. 2023. Mechanism of outer membrane destabilization by global reduction of protein content. Nature Communications 14(1), 9.

Min, S., Lee, H., Chae, D., Park, J., Lee, S.H., Oh, H.S., Lee, K., Lee, C.H., Chae, S. and Park, P.K. 2022. Innovative biofouling control for membrane bioreactors in cold regions by inducing environmental adaptation in quorum-quenching bacteria. Environ. Sci. Technol. 56(7), 4396-4403.

Nikkola, J., Liu, X., Li, Y., Raulio, M., Alakomi, H.-L., Wei, J. and Tang, C.Y. 2013. Surface modification of thin film composite RO membrane for enhanced anti-biofouling performance. Journal of Membrane Science 444, 192-200.

Overhage, J., Schemionek, M., Webb, J.S. and Rehm, B.H.A. 2005. Expression of the psl operon in *Pseudomonas aeruginosa* PAO1 biofilms: PslA performs an essential function in biofilm formation. Applied and Environmental Microbiology 71(8), 4407-4413.

Pourhassan, Z.N., Smits, S.H.J., Ahn, J.H. and Schmitt, L. 2021. Biotechnological applications of type 1 secretion systems. Biotechnology Advances 53.

Ren, L., Lu, Z., Xia, X., Peng, Y., Gong, S., Song, X., Jeppesen, E., Han, B.-p. and Wu, Q.L. 2022. Metagenomics reveals bacterioplankton community adaptation to long-term thermal pollution through the strategy of functional regulation in a subtropical bay. Water Res. 216.

Sheridan, E.A., Fonvielle, J.A., Cottingham, S., Zhang, Y., Dittmar, T., Aldridge, D.C. and Tanentzap, A.J. 2022. Plastic pollution fosters more microbial growth in lakes than natural organic matter. Nature Communications 13(1).

Shi, Y., Huang, J., Zeng, G., Gu, Y., Chen, Y., Hu, Y., Tang, B., Zhou, J., Yang, Y. and Shi, L. 2017. Exploiting extracellular polymeric substances (EPS) controlling strategies for performance enhancement of biological wastewater treatments: An overview. Chemosphere 180, 396-411.

Song, K., Xue, Y., Li, L., Deng, M. and Zhao, X. 2022. Impact and microbial mechanism of continuous nanoplastics exposure on the urban wastewater treatment process. Water Res. 223.

Sorasan, C., Edo, C., González-Pleiter, M., Fernández-Piñas, F., Leganés, F., Rodríguez, A. and Rosal, R. 2022. Ageing and fragmentation of marine microplastics. Science of the Total Environment 827, 9.

Sutrisna, P.D., Riadi, L., Buana, P.C.W., Khoiruddin, K., Boopathy, R., Wenten, I.G. and Siagian, U.W.R. 2023. Membrane and membrane-integrated processes for nanoplastics removal and remediation. Polymer Degradation and Stability.

Tamayo, L.A., Zapata, P.A., Vejar, N.D., Azócar, M.I., Gulppi, M.A., Zhou, X., Thompson, G.E., Rabagliati, F.M. and Páez, M.A. 2014. Release of silver and copper nanoparticles from polyethylene nanocomposites and their penetration into *Listeria monocytogenes*. Mater. Sci. Eng. C-Mater. Biol. Appl. 40, 24-31.

Teng, M., Zhao, X., Wang, C., Wang, C., White, J.C., Zhao, W., Zhou, L., Duan, M. and Wu, F. 2022. Polystyrene nanoplastics toxicity to zebrafish: Dysregulation of the brain -intestine-microbiota axis. Acs Nano 16(5), 8190-8204.

Vandana and Das, S. 2022. Genetic regulation, biosynthesis and applications of extracellular polysaccharides of the biofilm matrix of bacteria. Carbohydrate Polymers 291.

Wang, B., Zhang, L.F., Bae, S.C. and Granick, S. 2008. Nanoparticle-induced surface reconstruction of phospholipid membranes. Proceedings of the National Academy of Sciences of the United States of America 105(47), 18171-18175.

Wang, X., Jiang, C., Wang, D., Yang, Y., Fan, L., Xu, S. and Zhuang, X. 2023. Quorum sensing responses of activated sludge to free nitrous acid: Zoogloea deformation, AHL redistribution, and microbiota acclimatization. Water Res. 238.

Wang, X., Li, H., Chen, Y., Meng, X., Dieketseng, M.Y., Wang, X., Yan, S., Wang, B., Zhou, L. and Zheng, G. 2022. A neglected risk of nanoplastics as revealed by the promoted transformation of plasmid-borne ampicillin resistance gene by *Escherichia coli*. Environmental Microbiology 24(10), 4946-4959.

Wang, Y., Malkmes, M.J., Jiang, C., Wang, P., Zhu, L., Zhang, H., Zhang, Y., Huang, H. and Jiang, L. 2021. Antibacterial mechanism and transcriptome analysis of ultra-small gold nanoclusters as an alternative of harmful antibiotics against Gram-negative bacteria. Journal of Hazardous Materials 416.

Wen, J., Sun, H., Liu, Z., Zhu, X., Qin, Z., Song, E. and Song, Y. 2022. Aging processes dramatically alter the protein corona constitution, cellular internalization, and cytotoxicity of polystyrene nanoplastics. Environmental Science & Technology Letters 9(11), 962-968.

Weng, X., Mao, Z., Fu, H.-M., Chen, Y.-P., Guo, J.-S., Fang, F., Xu, X.-W. and Yan, P. 2022. Biofilm formation during wastewater treatment: Motility and physiological response of aerobic denitrifying bacteria under ammonia stress based on surface plasmon resonance imaging. Bioresource Technology 361.

Whiteley, M., Diggle, S.P. and Greenberg, E.P. 2018. Progress in and promise of bacterial quorum sensing research. Nature 555(7694), 126-126.

Wu, J., Liu, C., Wang, R., Yan, S., Chen, B. and Zhu, X. 2023. Enhanced bacterial adhesion force by rifampicin resistance promotes microbial colonization on PE plastic compared to non-resistant biofilm formation. Water Res. 242.

Xiong, X., Siddique, M.S., Graham, N.J.D. and Yu, W. 2022. Towards microplastics contribution for membrane biofouling and disinfection by-products precursors: The effect on microbes. Journal of Hazardous Materials 426.

Xu, F., Chen, P., Li, H., Qiao, S., Wang, J., Wang, Y., Wang, X., Wu, B., Liu, H., Wang, C. and Xu, H. 2021. Comparative transcriptome analysis reveals the differential response to cadmium stress of two *Pleurotus* fungi: *Pleurotus cornucopiae* and *Pleurotus ostreatus*. Journal of Hazardous Materials 416.

Xu, S., Wu, C., Guo, W.B., Yang, L.Y., Ji, R., Pan, K. and Miao, A.J. 2022. Polystyrene nanoplastics inhibit the transformation of tetrabromobisphenol a by the bacterium *Rhodococcus jostii*. Acs Nano 16(1), 405-414.

Yang, J., Monnot, M., Sun, Y., Asia, L., Wong-Wah-Chung, P., Doumenq, P. and Moulin, P. 2023. Microplastics in different water samples (seawater, freshwater, and wastewater): Removal efficiency of membrane treatment processes. Water Res. 232, 11.

Yang, X., Zhang, L., Chen, Y., He, Q., Liu, T., Zhang, G., Yuan, L., Peng, H., Wang, H. and Ju, F. 2022. Micro(nano)plastic size and concentration co-differentiate nitrogen transformation, microbiota dynamics, and assembly patterns in constructed wetlands. Water Res. 220.

Yu, C., Wu, J.J., Contreras, A.E. and Li, Q.L. 2012. Control of nanofiltration membrane biofouling by *Pseudomonas aeruginosa* using D-tyrosine. Journal of Membrane Science 423, 487-494.

Yu, L., Zhang, Q., Li, R., Qiao, B., Wang, Z., Zheng, L. and Peng, D. 2023. Extracellular polymeric substances trigger microbial immigration from partial denitrification (PD) to anammox biofilms in a long-term operated PD/anammox process in low-strength wastewater. Water Res. 229.

Zhai, Y., Guo, W., Li, D., Chen, B., Xu, X., Cao, X. and Zhao, L. 2024. Size-dependent influences of nanoplastics on microbial consortium differentially inhibiting 2, 4-dichlorophenol biodegradation. Water Res. 249, 121004.

Zhang, B., Yu, P., Wang, Z. and Alvarez, P.J.J. 2020a. Hormetic promotion of biofilm growth by polyvalent bacteriophages at low concentrations. Environ. Sci. Technol. 54(19), 12358-12365.

Zhang, C.Q., Brown, P.J.B., Miles, R.J., White, T.A., Grant, D.G., Stalla, D. and Hu, Z.Q. 2019. Inhibition of regrowth of planktonic and biofilm bacteria after peracetic acid disinfection. Water Res. 149, 640-649.

Zhang, M., He, L., Qin, J., Wang, S. and Tong, M. 2023. Influence of flagella and their property on the initial attachment behaviors of bacteria onto plastics. Water Res. 231.

Zhang, Q., Xia, T. and Zhang, C. 2020b. Chronic exposure to titanium dioxide nanoparticles induces commensal-to-pathogen transition in *Escherichia coli*. Environ. Sci. Technol. 54(20), 13186-13196.

Zhou, X.-X., He, S., Gao, Y., Li, Z.-C., Chi, H.-Y., Li, C.-J., Wang, D.-J. and Yan, B. 2021. Protein corona-mediated extraction for quantitative analysis of nanoplastics in environmental waters by pyrolysis gas chromatography/mass spectrometry. Analytical Chemistry 93(17), 6698-6705.